Anal. Bioanal. Electrochem., Vol. 15, No. 11, 2023, 967-987
https://www.doi.org/10.22034/abec.2023.709114

Analytical & Bioanalytical Electrochemistry

Full Paper

Corrosion Mitigation of Carbon Steel using Pyrazole Derivative: Correlation of Gravimetric, Electrochemical, Surface Studies with Quantum Chemical Calculations

L. Adlani,[1] N. Benzbiria,[2] A. Titi,[3] F. Benhiba,[4,5,*] I. Warad,[6] N. Timoudan,[5] G. Kaichouh,[5] A. Bellaouchou,[5] R. Touzani,[3] H. Zarrok,[1] H. Oudda,[1] and A. Zarrouk,[5,*]

[1]*Laboratory of Advanced Materials and Process Engineering, Faculty of Sciences, Ibn Tofail University, P.O. Box. 133, 14000 Kenitra, Morocco*
[2]*Laboratory of Interface Materials Environment, Faculty of Sciences Aïn Chock, Hassan II University, B.P. 5366 Maârif, Casablanca, Morocco*
[3]*Laboratory of Applied and Environmental Chemistry (LCAE), Mohammed First University, Oujda, Morocco*
[4]*Higher Institute of Nursing Professions and Health Techniques of Agadir, Annex Guelmim, Morocco*
[5]*Laboratory of Materials, Nanotechnology and Environment, Faculty of Sciences, Mohammed V University in Rabat, P.O. Box. 1014, Rabat, Morocco*
[6]*Department of Chemistry, AN-Najah National University, P.O. Box 7, Nablus, Palestine*

*Corresponding Authors, Tel.: +212665201397 (F. Benhiba); +212665201397 (A. Zarrouk)
E-Mails: benhibafouad@gmail.com (F. Benhiba); azarrouk@gmail.com (A. Zarrouk)

Received: 22 September 2023 / Received in revised form: 17 October 2023 / Accepted: 29 October 2023 / Published online: 30 November 2023

Abstract- The current paper revolves around the conduct of newly synthesized eco-friendly pyrazole derivative, N-((3,5 dimethyl-1H-pyrazol-1-yl)methyl)-4-nitroaniline (L5), as corrosion inhibitor for carbon steel (CS) in molar hydrochloric acid (1M HCl) solution. Both chemical and electrochemical techniques, namely weight loss measurements (WL), potentiodynamic polarization (PDP) and electrochemical impedance spectroscopy (EIS) were used to evaluate the efficiency of L5 molecule, as well as quantum-chemical methods. The organic compound was confirmed to be a good anti-corrosion compound with a maximum inhibition efficiency (IE%) of 95.1% at 10^{-3} M. In accordance to PDP outcomes, the inhibitor L5 acts as a mixed-type inhibitor. Assessment of the temperature influence evinces that L5 is chemisorbed on CS. The adsorption of L5 on CS surface appears to follow the Langmuir model. Scanning Electron Microscopy (SEM-EDX) and UV–visible disclose the constitution of a barrier film limiting the accessibility of corrosive ions into CS surface. Theoretical studies were

executed to support the results deriving from experimental techniques (WL, PDP and EIS). Furthermore, theoretical studies were carried out utilizing density functional theory (DFT) and molecular dynamics simulation (MDS) to investigate the most reactive locations of the L5 molecule and its adsorption process.

Keywords- Pyrazole derivative; Carbon steel; WL/PDP/EIS; SEM-EDX/UV-visible; Thermodynamic parameters; DFT/MDS

1. INTRODUCTION

Carbon steel holds a favorable position in several industries thanks to its excellent engineering properties. Yet, the metal suffers from a potent reactivity with its environment, inducing thus the demise of the material [1]. Metallic degradation occurs when metals and alloys are susceptible to reverting to their initial state as an oxide, sulfide, carbonate or other more stable salt upon the effect of environmental agents or chemical reagents [2]. To this day, many researchers have been conducting investigations of novel approaches, materials and potential technologies capable of retarding the deterioration of steel in aggressive media such as hydrochloric acid. Typically 15-28% HCl solutions are employed to finish several procedures such as acid cleaning, elimination of localized deposits, steel pickling and chemical washing [3,4]. A variety of anti-corrosion measures, such as improvement of materials, application of inhibitors, alloying, utilization of different forms of coatings, and the alteration of the environment, can drastically reduce the deterioration of metals [5]. Nevertheless, the simplest and cost-effective way to preclude metallic corrosion is the implementation of inhibitors [6,7]. Organic inhibitors, which tend to operate by adsorption (chemical or physical) to the metal surface, are more widely utilized to address this detrimental trend given their excellent biodegradability, ease of access, and eco-friendly character [8]. Other requirements for these organic compounds include prevention of metal breakdown, slowing down the action of acids, and stability at low concentrations [9,10]. Effective adsorption of organic inhibitors usually entails the presence of conjugate double bonds or π-electrons in triple and O, S, or N atoms in their structure [11].

Pyrazole compounds constitute a core category of heterocyclic products owing to their applicability in several areas. Indeed, during the past decades, numerous investigations have been conducted to elucidate the activity of pyrazole derivatives in corrosion mitigation in destructive acidic environments, for steel [12,13] as well as other metals and alloys [14,15]. In addition, the biological activity of pyrazoles, along with their usage as dyes, pesticides, insecticides, fungicides and herbicides have resulted in their widespread use [16–18]. It should be noted that the ability of suitable replacement with adequate functional groups renders pyrazoles highly relevant candidates in the creation of novel organic inhibitors. Regardless of the potent inhibitory properties of organic products, some are poisonous and raise health and environmental concerns. Hence, such challenges have initiated the development of new environmentally compliant corrosion inhibitors (EFCIs). As for the pyrazolic products, they

are considered as ecologically benign inhibitors as they show a strong chemical performance combined with good solubility in aggressive acid media, with respect to another class of organic compounds, a diminished level of toxicity and marginal environmental hazard [19,20]. Verma et al. [19] synthesized a pyrazolic product using microwave irradiation which exhibited an inhibition efficiency of 94.88% (IE) at 300 ppm in 1M HCl. The study conducted by Boudjellal et al. [21] on a pyrazolic carbothioamide compound showed its great prohibition activity in 1M HCl. Paul et al. [22] conducted an investigation on two carbohydrazide-pyrazole derivatives which presented notable mitigation capacity at 300 ppm in 15% HCl solution. Hameed et al. [23] carried out a study on a pyrazole molecule in 1M HCl which the IE exhibited a maximal value of 95%. Similar inhibition activity was stated by Elmsellem [24] who exploited a derivative comprising carbohydrazide and pyrazole in 1MHCl. As reported by Yadav [25], a pyrazolic derivative exhibited an impressive IE at a concentration of 250 ppm in 15% HCl.

Considering the aforementioned findings on pyrazole compound, a novel pyrzaole derivative, namely N-((3,5-dimethyl-1H-pyrazol-1-yl)methyl)-4-nitroaniline (L5), was synthesized while respecting the growing demand for biodegradable and sustainable compounds. L5 molecular structure was also precisely designed to exhibit a potent inhibition efficacy while taking into consideration L5 molar mass, which relates directly to its production cost. In view of the economic and ecological credentials of L5, the latter was inspected as corrosion inhibitor against the corrosion of carbon steel (CS) in molar HCl solution. A variety of both electrochemical and chemical methods were employed for this purpose. The morphology and nature of the protective film formed on CS surface was inspected using scanning electron microscopy (SEM-EDX). The UV-visible analysis was performed to gain insight of L5 inhibitor adsorption on the metallic surface. To acquire knowledge on the interactions and surface adsorption of L5 molecule, molecular dynamics simulations (MDS) were carried out.

2. EXPERIMENTAL SECTION

2.1. Materials

The metallic substrate used in the current paper consists of a CS bar having an elemental composition of (wt%); carbon (0.370), silicon (0.230), manganese (0.680), chromium (0.077), sulfur (0.016), titanium (0.011), nickel (0.059), cobalt (0.059), copper (0.16), and iron (remainder). Before immersion in the medium, metallic specimens of CS underwent a preparation process involving polishing by SiC paper having gradually finer particle sizes (from 150 to 1200). After a thorough cleansing with distilled water, acetone and air drying, CS samples were ready for further experiments.

2.2. Chemicals

Without any additional refinement, the compounds purchased from Sigma-Aldrich (Spain) were employed in their original state. Figure 1 depicts the structure of L5. The preparation of molar HCl solutions was carried out through diluting 37% analytical-grade HCl with double-distilled water. Corrosion trials were executed in a 1 M HCl solution devoid of inhibitor, and with various concentrations of L5 in the range of 10^{-3} M to 10^{-6} M. Electrochemical plots were drawn in an aerated environment without any stirring.

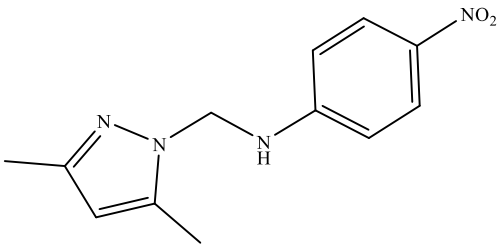

Figure 1. N-((3,5-dimethyl-1H-pyrazol-1-yl)methyl)-4-nitroaniline (L5)

2.3. Electrochemical apparatus and measurements

A saturated calomel electrode (SCE) serving as a reference electrode, a platinum wire acting as the counter electrode (CE), and a carbon steel as the working electrode (WE) were submerged in a classical Pyrex glass cell. The latter was filled with 90 cc of diluted hydrochloric acid to ensure complete immersion of the electrodes. The measurements were operated at typical ambient room temperature without any agitation, except for the research relying on the impact of temperature.

Through the use of a potentiostat Volta lab PGZ 100 connected to Voltamaster software, electrochemical tests and the corresponding curves and plots (Electrochemical Impedance Spectroscopy (EIS) and potentiodynamic polarization (PDP)) were collected. EIS data and PDP curves were exploited to assess the corrosion behavior of CS in both the absence and presence of L5 in 1M HCl.

For 30 minutes, the working electrode was immersed in the media under study to stabilize the open circuit potential (E_{OCP}). Afterwards, PDP trials were completed at a swipe rate of 5.10^{-4}V/s within the potential range of -0.8 V to -0.1 V. Prior to all testing, a stable state of voltage was established for a minimum of 30 minutes. The electrochemical studies were triple-realized for every L5 concentration, and the best plots were chosen for graphical representations.

The formula in Eq. (1) was used to compute the inhibitory efficiency (IE_{POL}(%)):

$$IE_{POL}(\%) = \frac{i_{corr} - i_{corr}(inhib)}{i_{corr}} \times 100 \qquad (1)$$

i_{corr} and i_{corr}(inhib) symbolize, respectively, the corrosion current densities in the presence and absence of inhibitive chemicals. A temperature range going from 303 to 333K was studied in a way to give further details on the temperature effect component.

Utilizing a similar workstation as the one previously mentioned above, EIS diagrams were drawn at E_{OCP} employing an AC signal with 10 mV amplitude and a frequency range of 10^5 to 10^{-2} Hz. Subsequently, the acquired plots were analyzed and adjusted in terms of an equivalent electrical model using ZView software version 3.4.

The formula expressed by Eq. (2) was used to determine the inhibitory efficiency using EIS:

$$IE_{EIS}\left(\%\right)=\frac{R_p\left(inhib\right)-R_p}{R_p\left(inhib\right)}\times 100 \qquad (2)$$

With $R_{P(inhib)}$ and R_P denote, respectively, the resistance of polarization post and prior to adding the inhibitor.

In a medium devoid of L5, we exploited the outcomes already published by our research team for both stationary and transient polarization methods for the influence of temperature and concentration, as measurements were conducted under similar conditions [26].

2.4. WL measurements

The weight loss (WL) of CS in the study media was measured in accordance with NACE/ASTM 169/G31-12a [27]. The prepared test solutions contain 100 ml of 1 M HCl concentration with 1, 0.1, 0.01 and 0.001 mM of L5 at 303 K. Firstly, CS substrates (2.0 ×2.0×0.1 cm^3) were subjected to a mechanical polishing treatment using abrasives of grades 400, 600, 800, 1000, and 1200 to obtain a mirror-like finish. Next, the plates were successively cleaned using water and ethanol as solvents. After accurate weighing and recording, the CS substrates were immersed in the test media for 6 hours at 303 K. Secondly, the CS plaques were taken out and the corrosive substances on their surface were rinsed off with demineralized water. Finally, the cleaned plates were air-dried, then weighed again to obtain the precise weights after corrosion. To calculate the inhibition efficiencies ($IE_W(\%)$) of L5 for CS in the experimental environment, Eq. (3) can be used [28]:

$$IE_W\left(\%\right)=\frac{W_0-W}{W_0}\times 100 \qquad (3)$$

where W_o and W are the WL of the CS in test media without and with L5, respectively.

2.5. UV-Vis. study

The potency and effectiveness of L5 inhibitor against CS corrosion was evaluated using the absorption UV-visible spectroscopy technique. The latter assesses the ability of the

inhibitor to absorb light at a specific wavelength. To this end, absorbance measurements were performed in absence and presence of a CS specimen at the specific concentration of 10^{-3}M of L5. The aim is to comprehend the interaction of L5 with the CS metallic surface in molar HCl solution. Wavelength scanning was extended from 200 to 600 nm through the use of a JASCO V-700 UV-Visible Spectrophotometer.

2.6. SEM-EDX explorations

Using the JEOL-JSM-IT-100 microscope, SEM micrographs of the CS surface have been acquired. With and without an inhibiting component, the ideal concentration of 10^{-3} M corrosive solutions was used. CS samples were individually exposed to the aforementioned medium for a period of 24 hours, gently removed, cleaned with high purity water, dried by air, and then examined. In the absence of inhibitor, we used SEM-EDS analysis in a work previously published [29].

2.7. DFT and MDS details

Based on the DFT approach carried out in the aqueous phase, attempts were made to understand the interaction mode of the pyrazol derivative on the CS surface [30]. This theoretical complement also aims to relate the experimentally assessed inhibitory activity of both neutral and protonated pyrazol analogues to their chemical responsiveness indices [31]. The Gauss. /09 software package was employed to optimize the molecular structure using the DFT/B3LYP/6-31++G (d, p) [32]. E_{LUMO}, E_{HOMO}, ΔE_{gap} (Eq. (4)), global hardness (Eq. (6)) «η», global electronegativity «χ» (Eq. (5)), and electrons transferred «ΔN_{110}» from occupied organic molecule orbitals to vacant orbitals of metal surface, with, the work function included in the Eq. 7 ($\Phi=\chi$(Fe110) =4.82 e) explain the theoretical value of χ in Fe (110) plan [33].

$$\Delta E_{gap} = E_{LUMO} - E_{HOMO} \tag{4}$$

$$\chi = \frac{1}{2}\left(E_{HOMO} + E_{LUMO}\right) \tag{5}$$

$$\eta = \frac{1}{2}\left(E_{HOMO} - E_{LUMO}\right) \tag{6}$$

$$\Delta N_{110} = \frac{\chi_{Fe_{110}} - \chi_{inh}}{2\left(\eta_{Fe_{110}} + \eta_{inh}\right)} = \frac{\Phi - \chi_{inh}}{2\eta_{inh}} \tag{7}$$

Molecular dynamics simulations (MDS) enable researchers to understand the interaction of L5 with Fe (110) arrangements. As in our previous work [34], the Forcite already found in Materials Studio/8 was a very important best model for this simulation.

The interactions of L5 and Fe(110) studied in the simulation box (27.30 * 27.30 * 37.13 $Å^3$) using the 491 H_2O, 9 H_3O^+,and 9 Cl^-. The temperature of the modeled unit was adjusted

using the Andersen thermostat at 303 K with a simulation time of "1000 ps" and the time step of "1.0 fs", all in the "COMPASS force" field [35].

3. RESULTS AND DISCUSSION

3.1. WL

3.1.1. Concentration effect

WLs represent an alternative efficient non-electrochemical method that involves subjecting the metal specimens in the investigated medium for a specified duration. The effect of inhibitor concentration on the inhibition activity was addressed firstly through weight loss (WL) assays of carbon steel (CS) electrode immersed during 6h in molar HCl medium in absence and presence of varying L5 concentration at T= 303 ± 2 K. The inhibition activity, IE_w(%), was calculated by Eq. (3) [28].

The WL descriptors divulged in Table 1 indicate that the percentage of inhibition activity (IE_W(%)) evolves significantly with concentration. The IE_W(%) value raises with incrementing L5 concentration. A maximal value of IE_W(%)=97.10 is exhibited at the optimized concentration of 10^{-3}M. The decline of corroding rate, in conjunction with an increment of the surface coverage (θ), infers that L5 adsorption on CS surface was improved by incrementing its concentration. Thereby, CS dissolution is substantially impeded through the hindrance of corrosion products formation.

Table 1. WL descriptors for CS electrode in 1M HCl medium in absence and presence of diverse concentrations of L5 at T = 303 ± 2 K

Medium	C (M)	W (mg/cm^2 h)	IE_W (%)	θ
Blank	1	2.880	-	-
L5	10^{-3}	0.084	97.1	0.971
	10^{-4}	0.259	90.9	0.909
	10^{-5}	0.456	84.0	0.840
	10^{-6}	0.627	78.0	0.780

3.1.2. Temperature effect

The weight loss trend and its respective inhibition action of CS sheet in the absence and presence of 10^{-3} M of L5 after 6 h of immersion at temperatures ranging from 303 to 333 K are disclosed in Table S1 (See SI file). A notable decline of *IE*w% with temperature increment is depicted, while the corrosion rate values raises with and without the presence of L5. The observed conduct can be related to the Coulomb interactions affecting significantly the

adsorption mode, while the Vander Waals interactions contribution prominently decreased regarding the adsorption energy of the {CS/1MHCl/10^{-3}M L5} system [36]. Therefore, it can be suggested that increasing the temperature affects negatively the interaction of L5 on CS surface which in turn subsides the inhibition activity. Note that several authors stated that temperature increment negatively impacts the chemical performance of the organic inhibiting compounds and induces accordingly their desorption from CS specimen [37]. The observed behavior is owed to the increase of surface roughness at higher temperatures disfavouring thus the adsorption of the inhibitory molecules on carbon steel [15].

Further details on the corrosion process were given through the evaluation of the kinetic activation parameters such as *E*a (activation energy), *ΔH*a* (activation enthalpy) and *ΔS*a* (activation entropy). These descriptors were assessed the examination of temperature influence as expressed by the Arrhenius law (Eq. (8)) and the Eyring-Polany formula (Eq. (9)) [28]:

$$W = A\exp\left(\frac{-E_a}{RT}\right) \tag{8}$$

$$W = \frac{RT}{Nh}\exp\left(\frac{\Delta S_a^*}{R}\right)\exp\left(\frac{\Delta H_a^*}{R}\right) \tag{9}$$

where *A* denotes the Arrhenius constant, *R* designates the gas constant, *T* represents the absolute temperature (K), *N* denotes the Avogadro's number and *h* stands for the Planck's constant. The respective plots are given in Figure S1 and Figure S2 in supplementary information file. The plotting of Ln(*W*) vs. (1000/*T*) depicts a straight line whose slope equals to $-E$a/*R*, which enables to estimate E_a value.

The following remarks can be deduced from the evaluation of Table S2 (See SI file):

- The corrosion processes must surpass an energetic barrier as disclosed by the positive value of ΔH_a* for both the blank and the medium inclosing L5 inhibitor. In other words, positive values of ΔH_a* reflect that CS dissolution process occurs as an endothermic reaction [38].

In molar HCl medium ΔS_a* is negative, whereas its value becomes positive with the addition of 10^{-3}M of L5. The observed trend points out the increment in disorder during the passage of the reagents to activated complex [38]. The activation energy of CS corrosion in 1M HCl containing L5 is greater compared to that in the inhibitor-free solution. Therefore, one may assume that the addition of the inhibitor L5 induces a rise of the energy barrier related to the corroding process. Expressly, the later will be further arduous on CS substrate and more repulsed due to the blockage of the surface-active centers by L5 molecules [28].

3.1.3. Adsorption isotherm

To examine the adsorption behavior of organic compounds upon a metal, it is mandatory to investigate different adsorption modes. In view of that, the surface coverage values (θ) were plotted to provide a fit for an appropriate adsorption isotherm. Tentative to several adsorption isotherms were carried out to ascertain the most suitable fit to the experimental outcomes.

As it is disclosed in Figure S3 (see supplementary information), the plotting of C/θ vs. C exhibited a line with a unitary slope and a linear correlation coefficient ~1. Accordingly, based on the outcomes of weight loss measurements, one may conclude that the Langmuir isotherm (monolayers adsorption) is more suitable to describe the adsorption of L5 on CS surface. Note that the formula expressing the Langmuir isotherm is denoted by the subsequent formula [28]:

$$\frac{C}{\theta} = \frac{1}{K_{ads}} + C \quad (10)$$

where K_{ads} denotes the adsorption/desorption equilibrium constant and C stands for L5 concentration in the medium.

An overview of the interaction of adsorption between the inhibitory compound and the metallic substrate can be derived through the evaluation of thermodynamic standard free energy of adsorption ΔG_{ads}. The latter was estimated from the equilibrium constant by the use of the subsequent relationship [7,28]:

$$\Delta G_{ads} = -RT\ln(55.5K) \quad (11)$$

where R designates the gas constant and T stands for the absolute temperature (K). The 55.5 value designates H_2O concentration in the solution (mol/L). As shown in Table S3 (in SI file), ΔG_{ads} value estimated from gravimetric data at 303K is -42.23 kJ mol^{-1}. Typically, ΔG_{ads} negative value evinces the stability of the protective layer developed by adsorption of L5 molecules on CS [38]. Within our case, ΔG_{ads} ~ -40 kJ/mol which corresponds to electron transfer between L5 and the metallic surface (chemisorption) along with the generation of coordination bonds [7,37].

3.2. Electrochemical investigation

3.2.1. PDP curves

To gain further insights into the corrosion kinetics of CS in 1 M HCl solution with and without varying concentrations of L5, PDP plots were drawn at stationary conditions, after 30 min of immersion at potential of corrosion (E_{corr}) and T=303 ± 2K. The obtained results are illustrated in Figure 2. The respective electrochemical kinetic descriptors, namely E_{corr}, corrosion current density (i_{corr}), the anodic Tafel slope (β_a) and cathodic Tafel slope (β_c), established through the extrapolation method, are displayed in Table 2. It is notable that the introduction of L5 into the corrosive solution gives arise to a prominent subsidence of both anodic and cathodic partial current densities. This may be the consequence of the mitigation of the anodic dissolution of the metallic surface and the cathodic H_2 production. In the cathodic branch, the graphs exhibit quasi-parallel lines, implying that the introduction of L5 to the investigated solution does not alter the process of H_2 generation. The reduction of H^+ on CS is predominantly carried out through charge transfer mechanism (pure activation process) [39].

From the analysis of Table, the values of i_{corr}, in the presence of varying concentrations of L5, are lower if compared to those assessed in the blank test solution. Moreover, E_{corr} values are slightly displaced towards more negative values with the introduction of L5 in the solution. As reported by Riggs [40], an organic product can be designated as anodic or cathodic behavior in case E_{corr} shifts at least 85 mV with respect to E_{corr} found in the acidic aggressive medium. As evinced by Table 2, the difference (ΔE_{corr}=20.3mV for the system {CS/1 M HCl/10^{-3}M L5}) is lower than 85 mV, confirming the mixed character of L5 [41]. Furthermore, the change in values of Tafel slopes (βa & βc) upon the addition of L5 indicates that the investigated inhibitor (L5) exhibits a tendency to reduce the specific surface area susceptible to corrosion and modify the corrosion process, likely through the blockage of CS surface reaction centers by L5 molecules [42].

It is worth to mention that the inhibition activity IE_{POL}(%) was assessed from PDP plots by Eq. (1). One can notice that increasing the concentration of L5 increases up the inhibition performance to a maximal value of IE_{POL}(%) = 93.6 for 10^{-3} M of L5. These results further substantiate that the adsorption of L5 on metal-electrolyte complex can proficiently block the active centers on CS surface and consequently prevents corrosion. The PDP outcomes support the favorable results obtained from weight loss measurements.

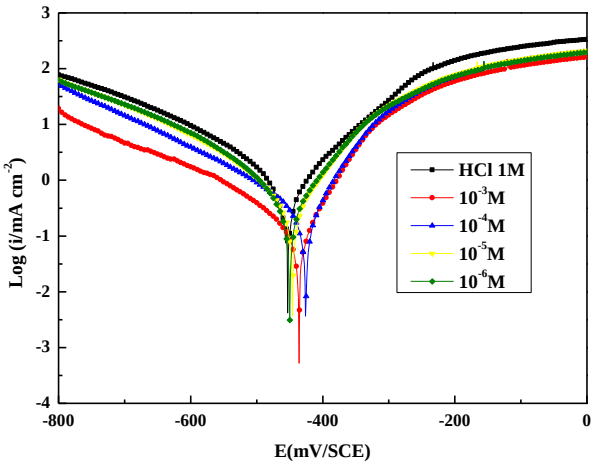

Figure 2. PDP plots for CS in 1M HCl in absence and presence of diverse concentrations of L5

Table 2. Potentiodynamic polarization descriptors for CS in 1MHCl (Blank) and with various L5 concentrations at T=303K (±0.5)

System	C (M)	$-E_{corr}$ (mV/SCE)	i_{corr} (µA cm^{-2})	β_a (mV dec^{-1})	$-\beta_c$ (mV dec^{-1})	IE_{POL} (%)
Blank	1	456.3	1104.1	112.8	155.4	---
L5	10^{-3}	436	70.4	50.1	78.2	93.6
	10^{-4}	422.3	152.6	48.5	94.7	86.1
	10^{-5}	445.3	233.6	62.1	82.9	78.8

	10^{-6}	449.2	285.9	70.6	85.8	74.1

3.2.2. EIS measurements

EIS is a powerful method often employed to disentangle the elemental processes purported to operate at the metal/solution interface and probe the adsorption of corrosion inhibitors. Figure 3 depicts the relevant Nyquist spectra drawn for the CS/1M HCl interface at E_{corr} in blank 1 M HCl as well as introducing diverse concentrations of L5 at 303±2K.

For all concentrations, Figure 3a depicts the occurrence of a unique flattened semi-circle accurately positioned on the center of the real part axis of the impedance Z_{re}. Note that the latter is consistent with the electrode polarization resistance R_p. It is commonly acknowledged that higher R_p values imply better performance of the inhibitor against corrosion. As L5 concentration progressively increases, the radius of the capacitive loops becomes wider. In the presence of L5 in the medium, enhanced polarization resistance (R_p) values are indicative that L5 can develop a dense anticorrosion film (mono or multilayer) on CS electrode surface, restraining hence the deterioration of the electrode effectively [36]. Moreover, the loops are characterized by a depressing semicircle at higher frequencies. In most of cases, the characteristic of this type of spectra may be assigned to the frequency dispersion owed to the roughness and heterogeneity of CS sample. For all concentrations of L5, the Nyquist diagrams display capacitive loops with an identical characteristic to those observed in the aggressive solution 1M HCl, possibly consistent with the electrical double layer. This demonstrates that the introduction of L5 into the medium does not affect significantly the corrosion process. The observed trend of EIS plots reveals that electron transfer is the limiting step in the corrosion pathway of the inspected system [35,37].

EIS data recorded for {1 M HCl/L5/CS} system was adjusted by the equivalent circuit depicted in Figure 3b, where R_e refers to the aqueous solution resistance, R_p designates the resistance of polarization, paralleling a constant phase element (*CPE*) referring to the capacitance of the electrical double layer (C_{dl}) at the interface CS/1 M HCl. The impedance function of a *CPE* (taking into account a non-ideal capacitive response on a heterogeneous surface) is described by Eq. (12):

$$Z_{CPE} = Q^{-1}(i\omega)^{-n} \quad (12)$$

where Q, i, ω, and n denote respectively the *CPE* constant, imaginary number (i^2=-1), angular frequency (ω=2πf), and phase shift. n designates the divergence with respect to the ideal conduct, comprised between 0 and 1. As claimed by Macdonald et al. [43], the value of n gives an indication on the substrate heterogeneity. For instance, n is homologous to a resistance when n=0, a capacitor for n=1, and assigned to a diffusion process in case n = 0.5.

The double capacitance values C_{dl} are determined using Eq. (13):

$$C_{dl} = (Q \times R_p^{1-n})^{1/n} \quad (13)$$

Table 3 gathers the corresponding EIS descriptors R_p, C_{dl}, and the inhibition efficiency IE_{EIS}%.

The evaluation of Table 3 evinces C_{dl} values continuously subside with the progressive addition of L5 at varying concentrations, which might be allocated to a lowering of local dielectric constant along with the CS electrode exposure and/or an overall increment in the electrical double-layer thickness [44]. In fact, it is concurred that the planar condenser model associates both the thickness of the protective layer (e) and C_{dl} as expressed by Eq. (14) [44]:

$$C_{dl} = \frac{\varepsilon_0 \times \varepsilon}{e} \times S \text{ (Helmoltz model)} \quad (14)$$

where e denotes the thickness of the depot, S represents the electrode area, ε_0 ($\varepsilon_0 = 8.8542\times10^{-14}$ F cm^{-1}) refers to the permittivity of vacuum and ε represents the relative dielectric constant. Thereby, the decrease of C_{dl} may be allocated to an enhancement of the metal coverage by L5 molecules. In other words, it can be deducted that the interactive L5 molecules adsorbed on CS substrate and gradually displaced H_2O molecules from CS surface, inducing thus in a decrease in the extent of CS dissolution [45].

In addition, the increment in n values with adding L5 into the medium, compared to the inhibitor-free electrolyte, might be associated with a depletion of the electrode surface coarseness [46]. The latter is likely the consequence of a barrier layer development on CS substrate.

Moreover, polarization resistance (R_p) values unveil a remarkable increase as L5 concentration increases. Although a unique time constant is depicted on Figure 3, it is noteworthy to indicate that R_p accounts for both charge transfer resistance R_{ct} and the protecting film resistance R_f (R_p=R_f+R_{ct}) when L5 is added to the solution. It may be suggested that the gradual addition of L5 into the aggressive solution enhances R_{ct} values as L5 concentration increases. This can be the result of the development of L5 protective film by adsorption on CS substrate, and thereby the delay of charge transfer process. Accordingly, the inhibition activity IE_{EIS}(%) value shows an increase with increasing inhibitory concentration (from 10^{-6} to 10^{-3} M). One may conclude then that L5 confers efficient protection against CS corrosion in molar HCl medium. These findings are consistent with WL and PDP results.

Table 3. Electrochemical impedance descriptors of CS in 1 M HCl solution comprising varied concentrations of L5 at 30 ±2 K

System	C (M)	R_s (Ω cm^2)	R_p (Ω cm^2)	$10^6\times Q$ ($\mu F\ s^{n-1}\ cm^{-2}$)	n	C_{dl} (μF cm^{-2})	IE_{EIS} (%)
Blank	1	0.83	21.7	293.9	0.845	115.6	----
L5	10^{-3}	1.01	444.1	71.3	0.883	45.1	95.1
	10^{-4}	0.95	203.6	130.7	0.876	78.2	89.3

	10^{-5}	0.91	124.3	187.8	0.861	102.4	82.5
	10^{-6}	0.87	90.7	219.1	0.852	110.9	76.0

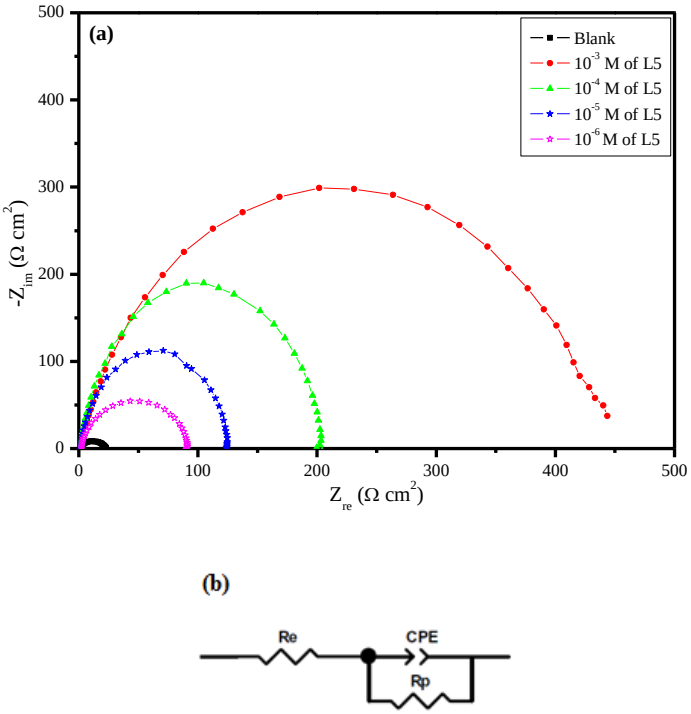

Figure 3. (a) Nyquist diagrams of CS in inhibitor free 1 M HCl solution and with the addition of various concentrations of L5 at 303 ± 2 K and (b) the corresponding electrical circuit employed for fitting EIS spectra

3.3. Surface analysis

Carbon steel specimens were inspected by SEM before immersion (Figure 4a), CS maintained immersed for 24 h in at 303 K in 1 M HCl without (Figure 4b) and with the introduction of 10^{-3} M of L5 (Figure 4c). The micrograph obtained in the inhibitor free solution (Figure 4b) shows that CS substrate is severely damaged as witnessed by the presence of grey aggregates. The related EDX spectrum depicts the occurrence of intense peaks of Cl and O atoms which may correspond likely to the presence of $FeCl_2$ and Fe_3O_4 as corrosion products [47]. This points out that carbon steel substrate undergoes general corrosion in 1M HCl. In medium enclosing L5 inhibitor, Figure 4c discloses that an adsorbed protective layer is developed on CS surface. The corresponding EDX spectrum discloses a peak of O atom (adsorption of L5), while the Cl peak contribution (mostly coming from the solution) is significantly diminished. These findings indicate that L5 has a great protective ability and prevents CS corrosion possibly by hindering aggressive ions access to its surface.

3.3. UV-Visible

To investigate the binding character of the organic species and Fe ions, UV–visible spectroscopic is exploited in many cases. It is reported that the shift in positioning of absorbance maximum and its value point out the development of a complex between two substances in an aqueous medium [37].

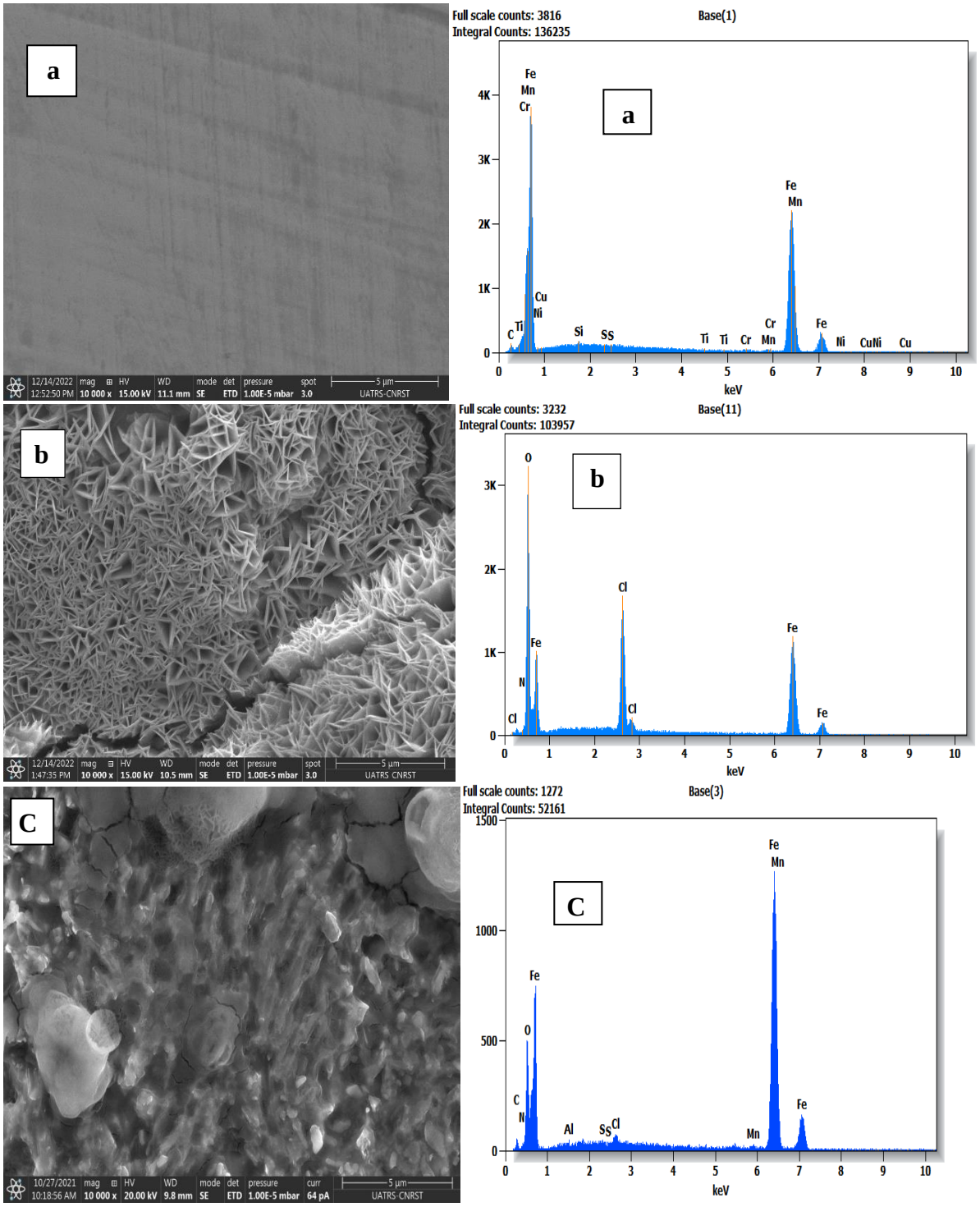

Figure 4. SEM micrographs and their corresponding EDX analysis of carbon steel specimens (a) before immersion, (b) after 24 h immersion in 1 M HCl and (c) 1 M HCl + 10^{-3} M of L5 at 303K

The probability of L5-Fe complex development was confirmed by the use of UV–visible absorption. The respective spectra of 1M HCl solution enclosing 10^{-3} M of L5, before and after 72h of immersion of CS, are depicted in Figure S4 in the supplementary file. The value of wavelength moves from 247 nm to 214 nm, additionally, another wave emerges at 258 nm indicating indeed a complex formation involving Fe^{2+} ions and L5 in the aggressive acidic solution [37].

3.5. DFT approach

The electronic capacities, global reactivity descriptors and local reactivity indices of the neutral (L5) and protonated ($L5H^+$) forms have been obtained in order to investigate the potency of corrosion inhibition and to identify a likely mechanism of action [48].

To better understand the reactivity of L5 in the protonated state, we have presented the results of the Marvin sketch software [49]. Figure S5 (see SI file) presents the variation of protonation % vs. pH. As analyzed in this Figure that the nitrogen atom hybridized sp^2 and included in the pyrazole ring protons with a high percentage, which results in a molecule positively charged as a cation ($L5H^+$).

To guarantee structural coherence, we need to be able to exclude imaginary frequencies at the same degree of theory. The structure, HOMO and LUMO of the L5 and $L5H^+$ molecules were plotted using GaussView/5 software.

Figure S6 (see SI file) depicts the energy-minimized structures, FMOs (HOMO-LUMO), and molecular electrostatic potential (MEP) of two neutral and protonated forms for L5 and $L5H^+$. The electronic representations of HOMO and LUMO show that the two forms studied had an almost total occupation except for some atomic part, which implies that the reactivity is very high with another species and especially with the carbon steel surface. Therefore, this distribution can induce parallel adsorption of these two forms with the Fe support.

The purpose of the E_{HOMO} and E_{LUMO} values is to measure the donor/acceptor ratio at the level of the molecule-metal relationship [50]. In this investigation of quantum computation, the behavior of the activity of the two considered neutral (L5) and charged ($L5H^+$) forms is followed by these two descriptors. Table 4 summarizes the data for the descriptors of L5 and $L5H^+$. The neutral molecule (L5) is more nucleophilic (E_{HOMO}=-6.176 eV) and the protonated molecule is more electrophilic (E_{LUMO}=-5.298 eV). ΔE_{gap} (E_{LUMO}-E_{HOMO}) is used to define the strength of a molecule's responsiveness, since the lower the value of this descriptor, the higher the specific responsiveness. The description comparison between the all values of this descriptor shows that the no charged form is more reactive with a low value of 4.187 eV.

The electronegativity presents an attractive power of the electrons of a chemical specie; the relevance of descriptor translates the reactivity of interaction [50]. It can be concluded from

Table 4 that the high value of the charged form $L5H^+$ (7.457 eV) implies that this form is more interactive and reactive with metal surface.

Indeed, the lower the hardness value (η), the greater the reactivity of a molecule and the more fruitful the interaction with a specific metal surface [50]. The value of 2.093 eV of L5 posted in Table 4 shows that this more reactive form.

The values of ΔN_{110} provide useful information on the tendency of the electrons to flow from the molecule to the CS surface ($\Delta N > 0$) or from the CS to the inhibitor ($\Delta N < 0$) [51]. Inspection of the ΔN_{110} data in Table 4 indicates that the electrons can flow from the neutral form ($\boldsymbol{\Delta N_{110}}$=0.176) to the CS surface. In contrast, $L5H^+$ does not show this attitude, which may be influenced by the cation of the N atom.

Table 4. Descriptors of the L5 and $L5H^+$

Forms	$\boldsymbol{E_{HOMO}}$ **(eV)**	$\boldsymbol{E_{LUMO}}$ **(eV)**	$\boldsymbol{\Delta E_{gap}}$ **(eV)**	$\boldsymbol{\chi}$ **(eV)**	$\boldsymbol{\eta}$ **(eV)**	$\boldsymbol{\Delta N_{110}}$
L5	-6.176	-1.989	4.187	4.082	2.093	0.176
$L5H^+$	-9.616	-5.298	4.318	7.457	2.159	-0.611

The adsorption pathway of L5 and $L5H^+$ on CS was investigated using Fukui function method, which enabled us to predict the nucleophilic (f_k^+) and electrophilic (f_k^-) attacks exerted by the most active sites of the two forms, and to enhance the experimental values [51]. This approach was carried out using the $Dmol^3$ method with the GGA correlation exchange functional and the DNP base as reported in the work published by Benhiba and al. [51].

Table 5. f_k^+ and f_k^- of the atoms for L5 and $L5H^+$ molecules

Atoms	f_k^- of L5	f_k^+ of L5	f_k^- of $L5H^+$	f_k^+ of $L5H^+$
C (1)	0.017	0.017	0.016	0.016
N (2)	0.033	0.033	0.001	0.068
N (3)	0.044	0.044	0.002	0.081
C (4)	0.059	0.059	0.015	0.104
C (5)	0.035	0.035	0.014	0.058
C (6)	0.050	0.049	0.001	0.102
C (7)	0.039	0.039	0.032	0.019
C (8)	0.025	0.025	0.050	0.009
C (9)	0.034	0.034	0.051	0.006
C (10)	0.022	0.022	0.047	0.001
C (11)	0.026	0.026	0.033	0.012
C (12)	0.027	0.028	0.039	0.018
N (13)	0.019	0.019	0.066	0.012
C (14)	0.018	0.018	0.007	0.029
C (15)	0.016	0.016	0.002	0.029
N (16)	0.048	0.048	0.046	0.013
O (17)	0.088	0.087	0.178	0.036

O (18)	0.088	0.088	0.180	0.034

The calculation data for two forms L5 and $L5H^+$ are listed in Table 5. For neutral form, the atoms bearing a high density of Fukui functions utilized such that the atoms, C(4), C(6), N(16), O(17) and O(18) for f_k^-; C(4), C(6), O(17) and O(18) for f_k^+, are responsible for the local reactivity and result in a greater number of available coordination bonds enhancing the adsorption of the inhibitor under study onto the metal support. For charged form, as observed in Table 5, the local reactivity arises and increases by the attractor effect due to the protonation, i.e. the attractor sites are very substantial.

3.6. MDS study

MDS are useful for predicting and understanding the adsorption profile of the L5 and $L5H^+$ molecules operate on the iron atomic support (Fe(110)) [52]. Figure 5 reproduces the best adsorption two forms onto the Fe(110) surface, respectively. As mentioned in these two views, the optimized pattern of the molecules takes up a substantial part of the Fe (110).

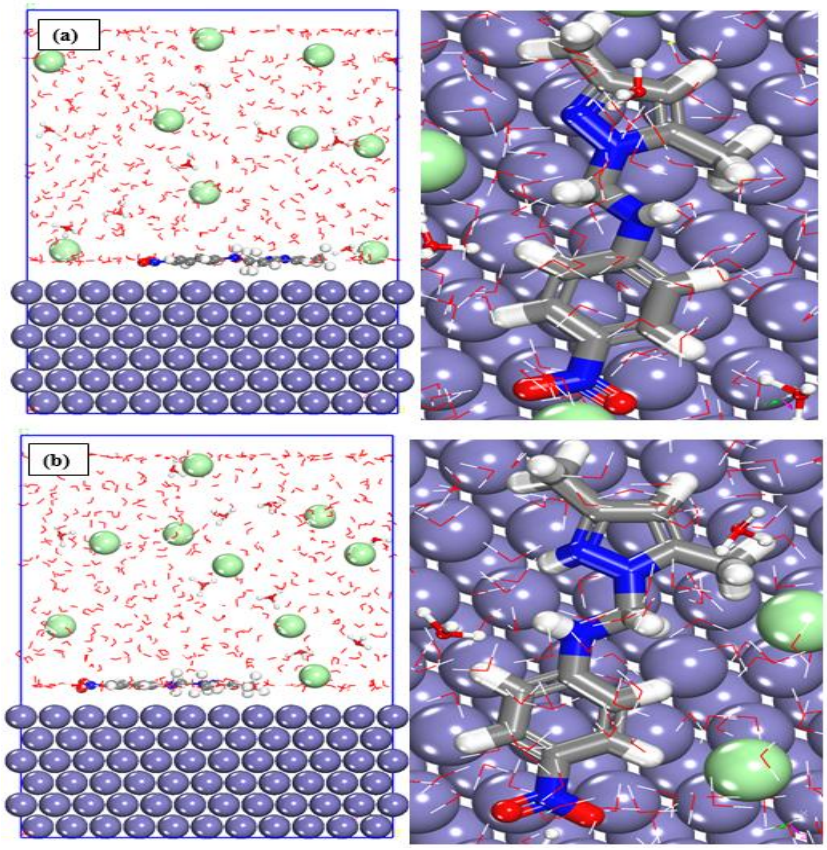

Figure 5. Side (left) and top (right) views of the L5/Fe(110) system **(a)** and of the $L5H^+$/Fe(110) system (b)

The $E_{interaction}$ (E_{inter}) value is defined by Eq. (15) [53]:

$$E_{inter} = - E_{(surface+ solution)} - E_{L5} + E_{total} \quad (15)$$

The low value of E_{inter} show the interactions of L5 and $L5H^+$ with the Fe(110) atoms [54]. The two values of the E_{inter} for the two systems are calculated and listed in Table S5 in the SI document, it appears from the comparative study that the most negative value of L5/Fe(110) (-782.712 kJ mol^{-1}) reflects a larger interaction. Therefore, the data from this simulation confirm the results obtained by DFT and the experimental study.

The "RDF" radial distribution function is the main objective of this new approach to assessing the adsorption aptitude for L5-Fe and $L5H^+$-Fe- interatomic distances [35]. The published literature confirmed that the likelihood of chemical adsorption was higher when the bond length was less than 3.5 Å. By contrast, physical adsorption is more probable [36]. In Figure S7 (see SI file), the spectral data from this method are illustrated. The peaks reveal that the L5-Fe and $L5H^+$-Fe are less than 3.5 Å.

3.7. Comparative study

In earlier studies, pyrazole derivatives have presented an outstanding potential as corrosion inhibitors in various media [12,13,55-59], mainly ascribed to their capability to develop a barrier layer on the metallic surfaces. Once incorporated into the corrosive medium, pyrazole molecules exhibit a good capacity to adhere to metals, and thus create a protective film which blocks the interaction between aggressive agents and the metal, and in turn mitigates corrosion process. Ongoing research on the inhibitory potential of pyrazoles, take into account several factors (molecular configuration, concentration of the compound, characteristics of the corrosive medium...). As shown in Table S6 (see SI file), previous researches report the good and satisfactory corrosion inhibition of CS by pyrazole derivatives in HCl solutions. In the current paper, our research highlights the simplicity of the synthesis of L5, the size of the molecular mass and the budget and ecological friendly attributes of L5. Besides, L5 exhibited a higher inhibition efficiency (95% for a concentration of 10^{-3} M) if compared to other pyrazole products (Table S6). Hence, based on the above, one may conclude that L5 is worth being considered as a convenient and efficient inhibitor for CS in molar HCl medium.

4. CONCLUSION

When the concentration of inhibitor rises, so does the ability to inhibit corrosion, and as the temperature falls, so does the effectiveness of inhibition. Results derived from PDP method showed that L5 compound is a mixed-type inhibitor. EIS measurements reveal that polarization resistance (RP) rises and double-layer capacitance (C_{dl}) falls. The adsorption of L5 on surface of carbon steel follows the Langmuir adsorption isotherm. The creation of a protective coating on the CS surface was revealed by SEM pictures. Theoretical approaches indicate a good adsorption of L5 and $L5H^+$ molecules on the selected surface.

Declarations of interest

The authors declare no conflict of interest in this reported work.

REFERENCES

[1] I.M. Chung, V. Hemapriya, S. H. Kim, K. Ponnusamy, N. Arunadevi, S. Chitra, M. Prabakaran, and M. Gopiraman, Chem. Eng. Commun. 208 (2021) 72.
[2] A. Abdel Nazeer, and M. Madkour, J. Mol. Liq. 253 (2018) 11.
[3] I. B. Obot, N. K. Ankah, A. A. Sorour, Z.M. Gasem, and K. Haruna, Sustain. Mater. Technol. 14 (2017) 1.
[4] L. O. Olasunkanmi, N. I. Aniki, A. S. Adekunle, L. M. Durosinmi, S. S. Durodola, O. O. Wahab, and E. E. Ebenso, J. Mol. Liq. 343 (2021) 117600.
[5] V. Saraswat, R. Kumari, and M. Yadav. J. Phys. Chem. Solids 160 (2022) 110341.
[6] D. K. Verma, M. Kazi, M. S. Alqahtani, R. Syed, E. Berdimurodov, S. Kaya, R. Salim, A. Asatkar, and R. Haldhar, J. Mol. Struct. 1241 (2021) 130648.
[7] N. Benzbiria, A. Thoume, S. Echihi, M. E. Belghiti, A. Elmakssoudi, A. Zarrouk, and M. Zertoubi, J. Mol. Struct. 1281 (2023) 135139.
[8] M. A. Migahed, M. M. EL-Rabiei, H. Nady, H. M. Gomaa, and E. G. Zaki , J. Bio Tribo. Corros. 5 (2019) 103.
[9] M. Rbaa, M. Galai, A. S. Abousalem, B. Lakhrissi, M. EbnTouhami, I. Warad, and A. Zarrouk, Ionics 26 (2020) 503.
[10] L. Guo, J. Tan, S. Kaya, S. Leng, Q. Li, and F. Zhang, J. Colloid Interface Sci. 570 (2020) 116.
[11] Y. E. Louadi, F. Abrigach, A. Bouyanzer, R.Touzani, A. El Assyry, A. Zarrouk, and B. Hammouti, Port. Electrochim. Acta 35 (2017) 159.
[12] B. A. Al Jahdaly, and G. S. Masaret, J. Mol. Liq. 364 (2022) 119933.
[13] M. S. Motawea, and M. A. Abdelaziz, Eur. J. Chem. 6 (2015) 342.
[14] A. Fouda, F. El-Taweel, and M. Elgamil, Int. J. Electrochem. Sci. 12 (12) (2017) 11397.
[15] E. Geler, and D. Azambuja, Corros. Sci. 42 (2000) 631.
[16] M. J. Naim, O. Alam, F. Nawaz, M. J. Alam, and P. Alam, J. Pharm. Bioallied Sci. 8 (2016) 2.
[17] M.J. Ahsan, H. Khalilullah, J. P. Stables, and J. Govindasamy, J. Enz. Inhib. Med. Chem. 28 (2013) 644.
[18] M. J. Alam, M. J. Ahsan, O. Alam, and S. A. Khan, Lett. Drug Des. Discov. 10 (2013) 776.
[19] C. Verma, V. S. Saji, M. A. Quraishi, and E. E. Ebenso, J. Mol. Liq. 298 (2020) 111943.
[20] H. S. Chandak, N. P. Lad, and D. S. Dange, Green. Chem. Lett. Rev. 5 (2012) 135.

[21] F. Boudjellal, H. B. Ouici, A. Guendouzi, O. Benali, and A. Sehmi, J. Mol. Struct. 1199 (2020) 127051.
[22] P. K. Paul, M. Yadav, and I. B. Obot, J. Mol. Liq. 314 (2020) 113513.
[23] R. S. Abdel Hameed, H. I. Al-Shafey, A. S. Abul Magd, and H. A. Shehata, J. Mater. Environ. Sci. 3 (2012) 294.
[24] R. Hsissou, H. Benassaoui, F. Benhiba, N. Hajjaji, and A. Elharfi, J. Chem. Technol. Metall. 52 (2017) 431.
[25] M. Yadav, R. R. Sinha, T. K. Sarkar, and N. Tiwari, J. Adhes. Sci. Technol. 29 (2015) 1690.
[26] W. Al Garadi, K. Jrajri, M. El Faydy, F. Benhiba, L. El Ghayati, N. K. Sebbar, E. M. Essassi, I. Warad, A. Guenbour, A. Bellaouchou, C. Jama, A. Alsalme, and A. Zarrouk, J. Indian. Chem. Soc. 99 (2022) 100742.
[27] J. Wen, X. Zhang, J. Chen, T. Liu, Y. Zhou, and L. Li, J. Ind. Eng. Chem. 107 (2022) 333.
[28] N. Mechbal, M. E. Belghiti, N. Benzbiria, C. H. Lai, Y. Kaddouri, Y. Karzazi, and M. Zertoubi, J. Mol. Liq. 331 (2021) 115656.
[29] E. H. Akroujai, S. Chetioui, N. Benzbiria, A. Barrahi, A. Chraka, A. Djedouani, S. Chtita, S. Lazar, I. Warad, A. Bellaouchou, M. Assouag, and A. Zarrouk, Int. J. Corros. Scale Inhib. 12 (2023) 1102.
[30] H. M. Abd El-Lateef, M. A. Abo-Riya, and A. H. Tantawy, Corros. Sci. 108 (2016) 94.
[31] T. Laabaissi, F. Benhiba, Z. Rouifi, M. Missioui, K. Ourrak, H. Oudda, Y. Ramli, I. Warad, M. Allali, and A. Zarrouk, Int. J. Corros. Scale Inhib. 8 (2019) 241.
[32] Y. Kharbach, F. Z. Qachchachi, A. Haoudi, M. Tourabi, A. Zarrouk, C. Jama, L. O. Olasunkanmi, E. E. Ebenso, and F. Bentiss, J. Mol. Liq. 246 (2017) 302.
[33] M. Oubaaqa, M. Ouakki, M. Rbaa, S. Ashraf, M. Abousalem, F. Benhiba, A. Jarid, M. Ebn Touhami, and A. Zarrouk, J. Mol. Liq. 334 (2021) 116520.
[34] M. Goyal, H. Vashisht, A. Kumar, S. Kumar, I. Bahadur, F. Benhiba, and A. Zarrouk, J. Mol. Liq. 316 (2020) 113838.
[35] H.C. Andersen, J. Chem. Phys. 72 (1980) 2384.
[36] M. G. Hosseini, M. Ehteshamzadeh, and T. Shahrabi, Electrochim. Acta 52 (2007) 3680.
[37] A. Thoume, D. Benmessaoud Left, A. Elmakssoudi, F. Benhiba, A. Zarrouk, N. Benzbiria, I. Warad, M. Dakir, M. Azzi, and M. Zertoubi, J. Mol. Liq. 337 (2021) 116398.
[38] A. Zarrouk, B. Hammouti, H. Zarrok, S. S. Al-Deyab, and M. Messali, Int. J. Electrochem. Sci. 6 (2011) 6261.
[39] R. Yıldız, Ionics 25 (2019) 859.
[40] O.L. Riggs Jr, Corrosion Inhibitors; Second ed. C.C. Nathan, T.X. Houston (1973).

[41] H. Zarrok, R. Saddik, H. Oudda, B. Hammouti, A. El Midaoui, A. Zarrouk, N. Benchat, and M. Ebn Touhami, Der Pharma Chem. 3 (2011) 272.
[42] V.V. Torres, R. S. Amado, C. F. de Sá, T. L. Fernandez, C. A. da Silva Riehl, A. G. Torres, and E. D'Elia, Corros. Sci. 53 (2011) 2385.
[43] D.D. MacDonald, NATO ASI Series (Series E: Applied Sciences), 203, Springer; Dordrecht. (1991).
[44] M. Abdallah, M. A. Hegazy, H. A. Ahmed, S. Arej, H. Al-Gorair, M. Hawsawi, F. Benhiba, I. Warad, and A. Zarrouk, RSC Adv. 12 (2022) 17050.
[45] M. Benoit, C. Bataillon, B. Gwinner, F. Miserque, M.E. Orazem, C.M. Sánchez-Sánchez, and V. Vivier, Electrochim. Acta 201 (2016) 340.
[46] M. El Faydy, F. Benhiba, H. About, Y. Kerroum, A. Guenbour, B. Lakhrissi, I. Warad, C. Verma, E.-S. M. Sherif, and E. E. Ebenso, J. Coll. Inter. Sci. 576 (2020) 330.
[47] M. M. Solomon, J. Colloid Interface Sci. 462 (2016) 29.
[48] A. Becke, J. Chem. Phys. 98 (1993) 5648.
[49] MarvinSketch Software. Version: 18.22, ChemAxon Ltd. (2018).
[50] R. Hamed, S. Jodeh, G. Hanbali, Z. Safi, A. Berisha, K. Xhaxhiu, and O. Dagdag, Front. Environ. Sci. 10 (2022) 977.
[51] F. Benhiba, R. Hsissou, K. Abderrahim, H. Serrar, Z. Rouifi, S. Boukhris, G. Kaichouh, A. Bellaouchou, A. Guenbour, H. Oudda, I. Warad, and A. Zarrouk, J. Bio Tribo. Corros. 8 (2022) 36.
[52] E. Alibakhshi, M. Ramezanzadeh, G. Bahlakeh, B. Ramezanzadeh, M. Mahdavian, and M. Motamedi, J. Mol. Liq. 255 (2018) 185.
[53] M. El Faydy, F. Benhiba, I. Warad, S. Saouabi, A. Alharbi, A.A. Alluhaybi, B. Lakhrissi, M. Abdallah, and A. Zarrouk, J. Mol. Struct. 1265 (2022) 133389.
[54] T. El-Mokadem, A. I. Hashem, N. E. A. Abd El-Sattar, E. A. Dawood, and N. S. Abdelshafi, J. Mol. Struct. 1274 **(**2023) 134567.
[55] G. Laadam, F. Benhiba, M. ElFaydy, A. Titi, A. S. AlGorair, M. Alshareef, H. Hawqawi, R. Touzani, I. Warad, A. Bellaouchou, A. Guenbour, M. Abdallah, and A. Zarrouk, Inorg. Chem. Commun. 145 (2022) 109963.
[56] K.H. Rashid, K. F. AL-Azawi, A. A. Khadom, A.S. Jasim, and M. M. Kadhim, J. Mol. Struct. 1287 (2023) 135661.
[57] G. Laadam, M. El Faydy, F. Benhiba, A. Titi, H. Amegroud, A. S. Al-Gorair, H. Hawsawi, R. Touzani, I. Warad, A. Bellaouchou, A. Guenbour, M. Abdallah, and A. Zarrouk, J. Mol. Liq. 375 (2023) 121268.
[58] K. Azgaou, M. Damej, S. El Hajjaji, N. K. Sebbar, H. Elmsellem, B. El Ibrahimi, and M. Benmessoud, J. Mol. Struct. 1266 (2022) 133451.
[59] S.M. Tawfik, J. Mol. Liq. 207 (2015) 185.